JOURNAL OF MATERIALS SCIENCE 26 (1991) 534–544

Microstructural refinement of β-sintered and Ti–6Al–4V porous-coated by temporary alloying with hydrogen

D. H. KOHN*, P. DUCHEYNE
Department of Bioengineering, University of Pennsylvania, Philadelphia, Pennsylvania 19104–6392, USA

A series of thermochemical treatments, in which hydrogen was used as a temporary alloying element to refine the lamellar microstructure of β-sintered and porous-coated Ti–6Al–4V was formulated. Each step of the treatment sequence (hydrogenation, eutectoid decomposition and dehydrogenation) was studied separately, on uncoated specimens and then on porous-coated specimens. The resultant microstructures can have α-grain sizes less than 1 μm, aspect ratios near unity and discontinuous grain boundary α (GBα), microstructural attributes which increase the fatigue strength. Microstructural refinement occurs because hydrogen-alloying reduces the $(\alpha + \beta) \leftrightarrow \beta$ transition temperature and enables a eutectoid decomposition reaction to occur. The optimal hydrogenation temperature is 850 °C, because hydrogen concentrations of 0.71 to 0.85 wt% are in-diffused and β-transformation is achieved. These weight percentages are in the optimal range for efficient eutectoid decomposition kinetics. β-transformation obviates the need for a separate β-transformation treatment step. A separate eutectoid decomposition treatment step may be used, or eutectoid decomposition may be combined with dehydrogenation. The finest eutectoid microstructures are obtained if hydrogen concentrations are in the range 0.5 to 0.8 wt%. The criteria for dehydrogenation are efficient removal of hydrogen, with minimal grain growth and absence of GBα. These criteria are best met by using dehydrogenation temperatures < 700 °C. Altering the sintering temperature or adding a porous coating does not affect the parameters of the hydrogen-alloying treatment steps.

1. Introduction

The structure–property relationships of titanium alloys have been studied in depth [1–6]. In general there are two classes of titanium alloy microstructures: equiaxed and lamellar. Following forging, thermal treatments below the $(\alpha + \beta) \leftrightarrow \beta$ transition temperature produce recrystallized microstructures having fine equiaxed grains, with a dispersion of β at primary α-grain boundaries. Equiaxed microstructures are characterized by small, rounded grains which have aspect ratios near unity. Thermal treatments above the $(\alpha + \beta) \leftrightarrow \beta$ transition temperature, followed by slow cooling into the $(\alpha + \beta)$ phase, produce an $(\alpha + \beta)$ lamellar microstructure. Lamellar microstructures are characterized by coarse α-platelets, forming α-colonies, and grain boundary α (GBα).

The mechanical properties of $(\alpha + \beta)$ titanium alloys are dictated by the amount, size, shape and morphology of the α-phase and the density of the α/β interfaces. Microstructures with a small (< 20 μm) α-grain size, a well-dispersed β-phase and a small α/β interface area yield the best high cycle fatigue strength [3, 7–9].

Many processing conditions result in the transformation of an equiaxed microstructure to a lamellar microstructure, and as a consequence a reduction in the high cycle fatigue strength. One important example is found in the field of orthopaedic and dental implantology. Implant fixation via bony ingrowth into a porous surface layer, sintered to a dense Ti–6Al–4V substrate, is potentially advantageous [10]. However, the porous coating and substrate are typically bonded by a β-sintering treatment, which transforms the equiaxed microstructure into a lamellar microstructure. A long-standing problem has been relieving the lamellar microstructure to improve the high cycle fatigue strength.

Until recently there was no efficient way to refine lamellar microstructures fully such that the fatigue strengths of the refined microstructures were equivalent to the fatigue strengths of equiaxed microstructures. However, the advent of treatments using hydrogen as a temporary alloying element has resulted in the creation of a unique class of microstructures which are finer than equiaxed microstructures and superior in tensile and fatigue strength [9, 11–16]. The

* *Present address*: Department of Biologic and Materials Sciences, 2213 School of Dentistry, The University of Michigan, Ann Arbor, Michigan 48109–1078, USA.

0022–2461/91 $03.00 + .12

key step in the treatment sequence is a eutectoid decomposition reaction, in which eutectoid α nucleates from the prior β-grains [11]. A eutectoid decomposition occurs because hydrogen lowers the $(\alpha + \beta) \leftrightarrow \beta$ transformation temperature, making phase transformation more favourable thermodynamically. Kerr *et al.* [11] showed that eutectoid decomposition and microstructural refinement are kinetically optimized if hydrogen concentrations are in the range 0.6 to 1.0 wt % and eutectoid decomposition is carried out at 590 °C.

Hydrogen-alloying treatments have successfully transformed the microstructure and increased the fatigue strength of cast [9, 12–14], powder [12–14, 17] and mill annealed Ti–6Al–4V [11, 13, 14], but the phase transformations which produce hydrogen-alloy treated microstructures have not been fully characterized. The objectives of this research were first, to formulate a series of hydrogen-alloying treatments which could refine the lamellar microstructure of β-sintered and porous-coated Ti–6Al–4V (commercially pure titanium powdered spheres sintered to dense Ti–6Al–4V) and, secondly to characterize the material and experimental parameters controlling the phase transformations and microstructural refinement. Each step of the treatment sequence was studied separately, on uncoated specimens and then on porous-coated specimens. The specific objectives of each treatment step (hydrogenation, eutectoid decomposition and dehydrogenation) were, respectively, to determine which temperature(s) and time(s) yielded hydrogen concentrations in the optimal range, to determine the extent of microstructural refinement for different eutectoid decomposition treatments and to determine dehydrogenation parameters which could first, reduce hydrogen concentrations to levels below 0.012 wt % and, secondly, maintain the refined microstructure produced during eutectoid decomposition.

2. Methods and materials

The material used for the thermochemical treatments was 15.6 mm diameter forged, annealed, extra-low interstitial (ELI) grade Ti–6Al–4V rod material. The chemical composition (Table I) conformed to ASTM F136-84 [18].

Specimens 62.5 mm long were β-sintered (1100 °C for 0.5 h), in a microprocessor-controlled vacuum furnace (BREW 466S, Concord, New Hampshire, USA), at vacuum pressures of 10^{-5} to 10^{-6} torr, to create a lamellar microstructure.

2.1. Hydrogenation and β-transformation

Two to four specimens per treatment were hydrogenated at 575, 650, 725 or 800 °C for 0.5, 1 or 2 h, and at 850 °C for 0.5 or 2 h. Hydrogenation was performed in an enclosed hydroxyl quartz tube (900 mm length × 37.5 mm diameter) which was mounted in a laboratory furnace (Sandland, Newark, New Jersey, USA). After inserting the specimens, the tube was sealed to prevent any gas leaks. An argon tank was connected to the gas lines, as a backup reservoir in case primary gas flow decreased or stopped. All gases passed through a gas purifier before entering the tube, to limit contamination, and dummy specimens were placed closest to the gas source to act as getter materials.

The quartz tube was first purged with argon, at a flow rate of 10 standard cubic feet per hour (SCFH) (0.28 $m^3 h^{-1}$), for 30 min. Hydrogen was then introduced at 10 SCFH. The partial pressure of all gases used in this study was 1 atm (101 kPa). The partial pressure was controlled by adjusting a valve on the gas line and the flow rate was controlled by a Brooks flowmeter. Once a steady hydrogen flow was established, the specimens were heated to the hydrogenation temperature at a rate of 20 to 25 °C min^{-1}. After the hydrogenation temperature was reached, the hydrogen flow rate was increased to 20 SCFH. Excess gas was released through an oil bubbler and burned off in a Bunsen burner. Temperature was monitored with two chromel–alumel thermocouples, each placed adjacent to a specimen lying at one end of the hot zone of the furnace.

After hydrogenation, argon flow was introduced at a flow rate of 10 SCFH. The flow rate was lowered to 2.5 SCFH when all residual hydrogen was bled from the gas line, and specimens were allowed to cool to room temperature. The quartz tube was repositioned so the region in which the specimens rested was outside of the hot zone of the furnace. Shifting the quartz tube allowed for a more rapid (30 °C min^{-1}) and uniform cooling, and minimized hydrogen loss due to out-diffusion.

The concentration of hydrogen that diffused into Ti–6Al–4V was determined by weighing the specimens to the nearest 0.1 mg before and after hydrogenation. Optical microscopy and scanning electron microscopy (SEM) were used to investigate the microstructures and surfaces of the hydrogenated specimens.

2.2. Eutectoid decomposition

Hydrogenation–β-transformation and eutectoid decomposition were performed consecutively in the same furnace. Following a hydrogenation treatment of 850 °C for 0.5 h, specimens were cooled (3.5 °C min^{-1}) to a eutectoid temperature of 590 °C in either an argon or a hydrogen environment, at a flow rate of 10 SCFH. Eutectoid treatments, in argon or hydrogen

TABLE I Chemical composition of as-received Ti–6Al–4V rod material

	Nitrogen	Carbon	Hydrogen	Iron	Oxygen	Boron	Copper	Silicon	Aluminium	Vanadium
wt %	0.018	0.014	0.009	0.16	0.12	0.001	0.002	0.13	6.1	4.2

Chemical analysis and mechanical data supplied by Titanium Metals Corporation of America, Henderson, Nevada, USA.

environments, lasted 2 or 4 h, and specimens were then cooled to room temperature in an argon atmosphere, in the same manner as described above.

To uncouple the effects of cooling from the hydrogenation temperature to the eutectoid temperature from the effects of the eutectoid treatment itself, a group of specimens was hydrogenated and cooled to 590 °C. The specimens were then immediately cooled to room temperature, without undergoing a eutectoid treatment.

After each eutectoid decomposition treatment, specimens were weighed to determine changes in hydrogen concentration. Eutectoid transformation and microstructural refinement were evaluated microscopically.

2.3. Dehydrogenation

Cylindrical specimens that underwent hydrogenation (850 °C for 0.5 h) and eutectoid decomposition (590 °C for 2 or 4 h in argon) treatments were sectioned into discs 5 mm thick. Two discs from each treatment were dehydrogenated in vacuum at 600; 650, 750 or 800 °C for 2 h or at 700 °C for 0.5, 1 or 2 h. Two specimens from each treatment also underwent two-step hydrogenation–dehydrogenation cycles of 850 °C for 0.5 h/600 °C for 8 h or 850 °C for 0.5 h/700 °C for 2 h. Following dehydrogenation, discs from each treatment group were also vacuum annealed at a higher temperature (925 °C for 4 h), to determine whether any residual hydrogen remained.

The following dehydrogenation treatments were performed on full cylindrical specimens: (a) 600 °C for 8, 16 or 24 h and 650 °C for 8 or 16 h, (b) 775 °C for 4 h and (c) 800 °C for 2 h. All three dehydrogenation treatments were preceded by a hydrogenation treatment of 850 °C for 0.5 h and treatments (b) and (c) were also preceded by a hydrogenation–eutectoid decomposition treatment of 850 °C for 0.5 h/590 °C for 4 h in argon.

Dehydrogenation was performed in a vacuum furnace (Vac Aero model VAH-1212-2600). The furnace was evacuated initially to 10^{-6} to 10^{-7} torr and maximum pressures of 10^{-4} to 10^{-5} torr were maintained during dehydrogenation. After dehydrogenation, specimens were furnace-cooled to room temperature.

Specimens were then weighed to determine the extent of hydrogen evolution. Hydrogen gas concentrations were also measured by a carburizing fusion technique (CFT; Alpha Resources, Stevensville, Michigan, USA), to serve as a comparison with the hydrogen concentrations determined by weighing. Metallographic analysis determined the extent of grain growth during dehydrogenation, and effective α-grain sizes were measured using a modified intercept procedure [19].

2.4. Effect of sintering temperature, porous coating and thermal cycle

To determine whether there was a difference in the resultant microstructures between smooth and porous-coated specimens following each step of the hydrogen-alloying treatment sequence, porous-coated specimens underwent: (a) hydrogenation (850 °C for 0.5 h) or (b) hydrogenation–eutectoid decomposition (850 °C for 0.5 h/590 °C for 4 h in argon). Porous-coated specimens, which were sintered at 1370 °C for 4 h, had a coarser lamellar microstructure than the specimens sintered at 1100 °C. Therefore, a group of uncoated cylindrical control specimens was also sintered at 1370 °C and subjected to treatments (a) and (b).

A group of uncoated specimens was also treated according to (a) and (b), but only in an argon environment. Evaluating samples treated with a hydrogen-alloying cycle without hydrogen allowed the effects of the thermal treatments to be distinguished from the effects of the hydrogen.

3. Results

3.1. Hydrogenation

Bulk concentrations of hydrogen are listed in Table II. These results were obtained by weighing specimens to the nearest 0.1 mg before and after hydrogenation and then correcting for two factors. First, the interstitial hydrogen concentration in the as-received material was 0.009 wt % (Table I) and, secondly, treatments without hydrogen showed the maximum weight gain due to diffusion of other elements to be 0.030 wt %. Therefore, 0.021 wt % was subtracted from the measured weight percentages as a combined correction factor. The microstructures following β-sintering and hydrogenation at 725, 800 and 850 °C are shown in Figs 1 and 2.

3.2. Eutectoid decomposition

Table III lists the different eutectoid treatments performed and the resultant hydrogen concentrations. Representative microstructures following eutectoid

TABLE II Hydrogen concentrations in Ti–6Al–4V cylinders following hydrogenation

Hydrogenation treatment	Hydrogen (wt %)
575 °C for 0.5 h	1.01 (0.06)
575 °C for 1 h	1.54 (0.07)
575 °C for 1 h[a]	1.56 (0.06)
575 °C for 2 h	1.61 (0.09)
650 °C for 0.5 h	1.03 (0.00)
650 °C for 1 h	1.38 (0.15)
650 °C for 2 h	1.36 (0.01)
725 °C for 0.5 h	1.02 (0.09)
725 °C for 1 h	1.16 (0.02)
725 °C for 2 h	1.09 (0.03)
800 °C for 0.5 h	0.82 (0.03)
800 °C for 0.5 h[a]	0.76 (0.01)
800 °C for 1 h	0.85 (0.01)
800 °C for 2 h	0.81 (0.07)
850 °C for 0.5 h	0.74 (0.05)
850 °C for 0.5 h[a]	0.45 (0.04)
850 °C for 2 h	0.71 (0.04)

Figures in parentheses are standard deviations. Nominal cooling rate 30 °C min^{-1}.
[a] Cooling rate 3.5 °C min^{-1}.

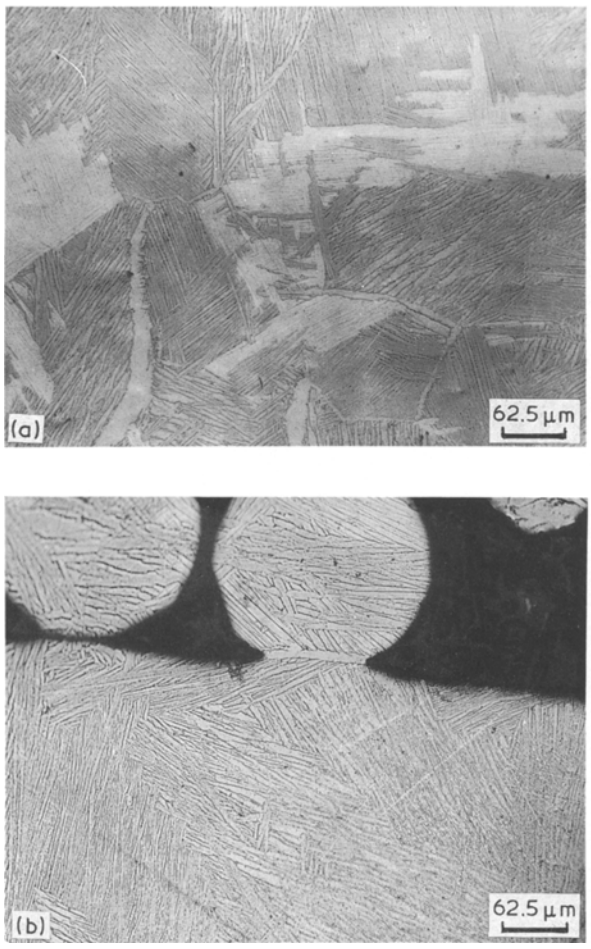

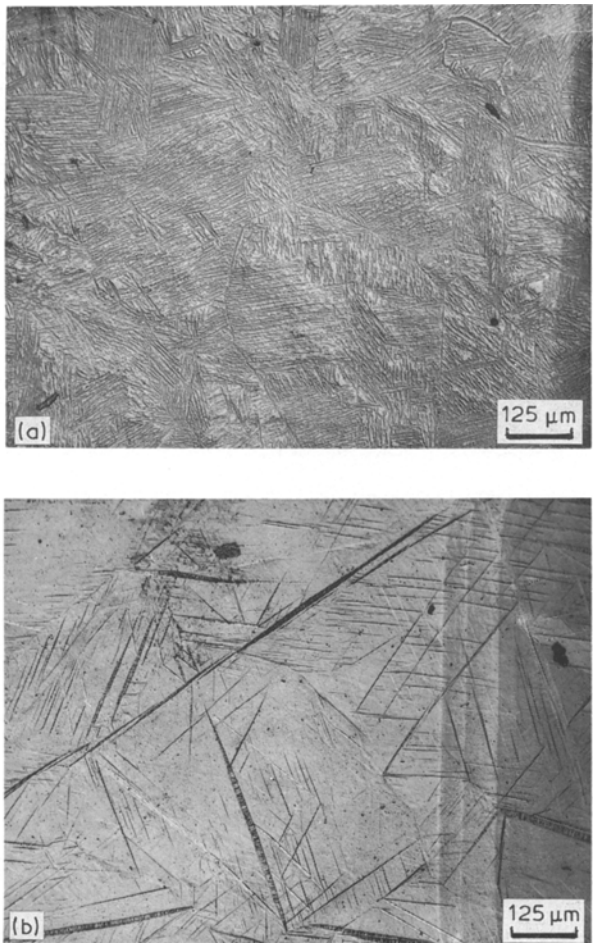

Figure 1 Light micrographs of lamellar Ti–6Al–4V: (a) uncoated and (b) porous coated.

decomposition in hydrogen and argon atmospheres are shown in Figs 3 and 4.

3.3. Dehydrogenation

The total concentration of hydrogen removed from the discs (Table IV) was the sum of the hydrogen concentrations removed during the two vacuum annealing treatments. The calculated weight losses were consistently 0.49 to 0.50 wt %, verifying that the hydrogen concentrations calculated based on weight differences remaining after dehydrogenation were accurate and that hydrogen concentrations were constant throughout any specimen.

The average hydrogen concentrations remaining in the cylinders after dehydrogenation are listed in Table V.

The microstructures following dehydrogenation are shown in Fig. 5. Table VI lists the average α-grain size for three dehydrogenation treatments which resulted in acceptable residual hydrogen levels. The complete treatment sequences, referred to respectively as HAT-1, HAT-2 and HAT-3, were (a) hydrogenation (850 °C for 0.5 h)–dehydrogenation (650 °C for 16 h), (b) hydrogenation (850 °C for 0.5 h)–eutectoid decomposition (590 °C for 4 h)–dehydrogenation (800 °C for 2 h) and (c) hydrogenation (850 °C for 0.5 h)–eutectoid decomposition (590 °C for 4 h)–dehydrogenation (775 °C for 4 h).

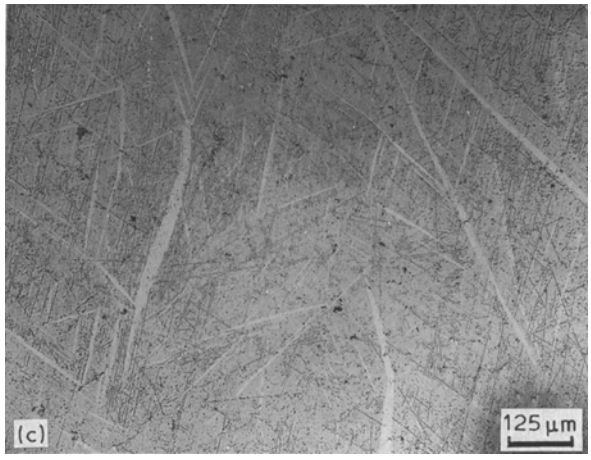

Figure 2 Light micrographs of β-sintered Ti–6Al–4V following hydrogenation treatments of (a) 725 °C for 0.5 h, (b) 800 °C for 0.5 h and (c) 850 °C for 0.5 h. Hydrogenation at 850 °C resulted in a fully transformed β_H microstructure.

TABLE III Hydrogen concentrations following hydrogenation at 850 °C and eutectoid decomposition treatments

Eutectoid decomposition treatment	Hydrogen (wt %)
590 °C for 2 h/hydrogen	1.68
590 °C for 4 h/hydrogen	1.84
590 °C for 2 h/argon	0.50
590 °C for 4 h/argon	0.50
590 °C for 8 h/argon	0.35
590 °C for 0 h/argon	0.50

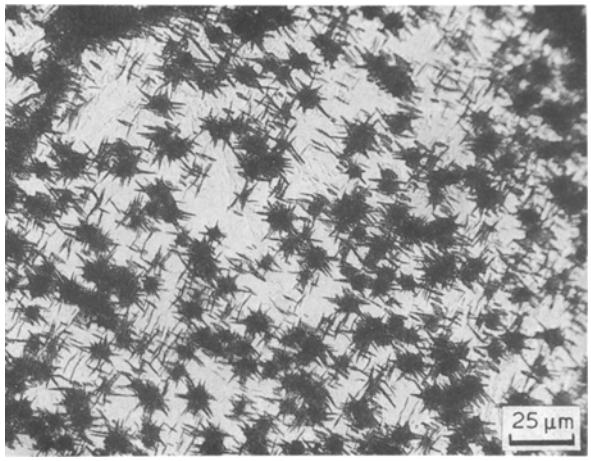

Figure 3 Light micrograph of Ti–6Al–4V following β-sintering, hydrogenation treatment of 850 °C for 0.5 h and eutectoid decomposition treatment of 590 °C for 4 h in hydrogen, showing "black plates".

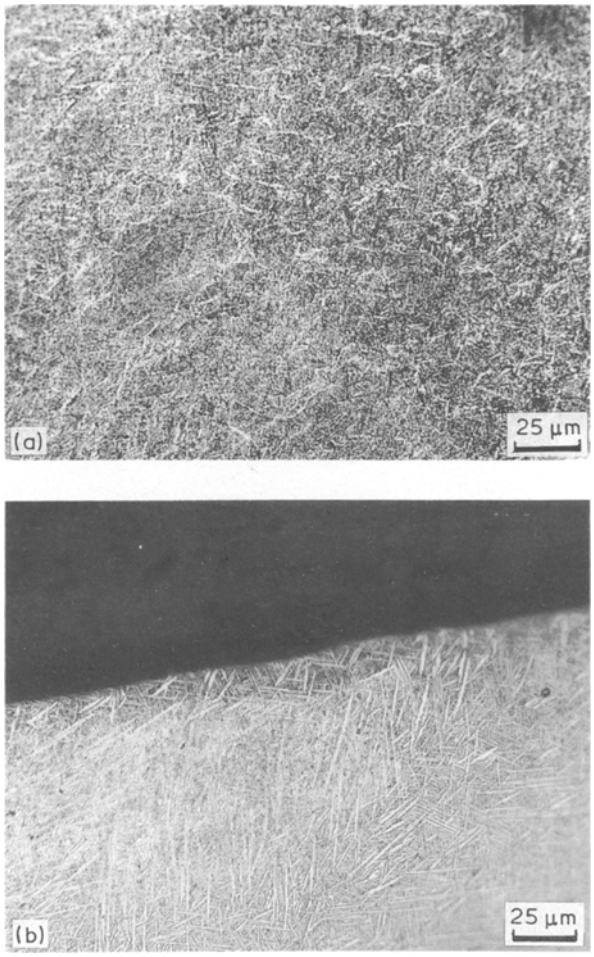

Figure 4 Light micrographs of Ti–6Al–4V following β-sintering, hydrogenation treatment of 850 °C for 0.5 h and eutectoid decomposition treatments of (a) 590 °C for 4 h in argon and (b) 590 °C for 8 h in argon, showing precipitation of eutectoid-α.

3.4. Effect of sintering temperature and porous coating

The results of a parametric study on the effect of sintering temperature and porous coating on the hydrogen-alloying treatment steps are listed in Table VII.

Microstructures obtained following each of the steps in the hydrogen-alloying treatment sequence performed on porous-coated samples are shown in Fig. 6.

TABLE IV Hydrogen concentrations remaining in Ti–6Al–4V discs following dehydrogenation

Treatment	Hydrogen (wt %)	Hydrogen following 925 °C for 4 h (wt %)
600 °C for 2 h	0.163 (0.001)	0.002 (0.003)
600 °C for 8 h	0.03 –	– –
650 °C for 2 h	0.079 (0.005)	0.002 (0.003)
700 °C for 0.5 h	0.058 (0.007)	0.008 (0.000)
700 °C for 1 h	0.038 (0.004)	0.001 (0.001)
700 °C for 2 h	0.018 (0.011)	0.007 (0.007)
750 °C for 2 h	0.017 (0.009)	0.013 (0.007)
800 °C for 2 h	0.006 (0.005)	0.005 (0.006)

Figures in parentheses are standard deviations.

TABLE V Hydrogen concentrations remaining in Ti–6Al–4V cylinders following dehydrogenation

Dehydrogenation treatment	Average hydrogen: weighing (wt %)	Average hydrogen: CFT (wt %)
600 °C for 8 h	0.0754 (0.0072)	–
600 °C for 16 h	0.0327 (0.0064)	0.0255 (0.0030)
600 °C for 24 h	0.0357 (0.0058)	–
650 °C for 8 h	0.0236 (0.0000)	–
650 °C for 16 h	0.0089 (0.0024)	–
775 °C for 4 h	0.0196 (0.0064)	0.0051 (0.0026)
800 °C for 2 h	0.0167 (0.0010)	–

Figures in parentheses are standard deviations.

4. Discussion

4.1. Hydrogenation

Controlled hydrogenation is necessary for the successful completion of each treatment step. As the hydrogenation temperature increased, the total hydrogen indiffusion decreased and hydrogen reached an equilibrium concentration more rapidly (Table I). These trends are predicted by diffusion theory [20] using diffusion coefficients for titanium [21].

Hydrogenation at 800 to 850 °C consistently yielded hydrogen concentrations of 0.71 to 0.85 wt %, values which are in the range considered optimal from the point of view of eutectoid decomposition kinetics [11]. At 800 and 850 °C hydrogen concentrations were independent of the hydrogenation time, indicating that hydrogen saturation occurred and a uniform hydrogen distribution was achieved. Hydrogen uniformity produced uniform microstructural refinement in the subsequent treatment steps and minimized the scatter in mechanical properties [16].

Cooling at a rate of 3.5 °C min^{-1} following hydrogenation at 850 °C resulted in a mean hydrogen concentration of 0.45 wt %. This concentration is below the minimum concentration necessary for optimal eutectoid transformation. At temperatures > 500 °C, out-diffusion of hydrogen can occur during cooling. Hydrogen concentrations were independent of the cooling rate for hydrogenation temperatures < 800 °C, since the temperature interval in which out-diffusion occurred was limited.

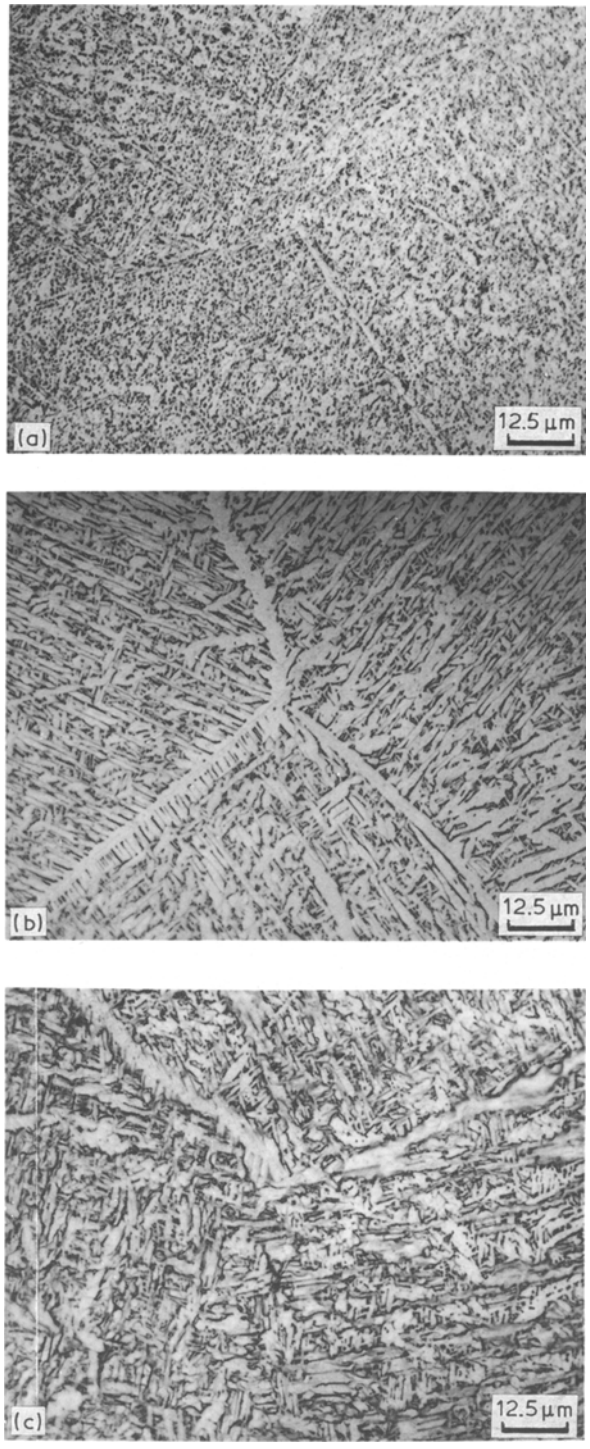

Figure 5 Light micrographs of β-sintered Ti–6Al–4V subjected to (a) HAT-1: hydrogenation–dehydrogenation treatment of 850 °C for 0.5 h in hydrogen/650 °C for 16 h in vacuum, (b) HAT-2: hydrogenation–eutectoid decomposition–dehydrogenation treatment of 850 °C for 0.5 h in hydrogen/590 °C for 4 h in argon/800 °C for 2 h in vacuum and (c) HAT-3: hydrogenation–eutectoid decomposition–dehydrogenation treatment of 850 °C for 0.5 h in hydrogen/590 °C for 4 h in argon/775 °C for 4 h in vacuum.

Too slow a cooling rate can therefore reduce the hydrogen concentration to below the optimal concentration for eutectoid transformation and result in the formation of acicular-α. Too rapid a cooling rate can result in cracking [22]. Therefore, moderate cooling rates of approximately 30 °C min^{-1} should be used. The decision of which cooling rate to use may be avoided altogether, by employing consecutive cycles of hydrogenation and eutectoid decomposition,

TABLE VI Average α-grain size for different Ti–6Al–4V microstructures

Microstructure	Average α-grain size (μm)
Equiaxed	3.40 (0.51)
Lamellar	4.00 (1.57)
HAT-1	0.91 (0.07)
HAT-2	1.17 (0.06)
HAT-3	1.26 (0.29)

Figures in parentheses are standard deviations.

TABLE VII Effect of porous coating and sintering temperature on hydrogen-alloying treatments

(I) Effect of sintering temperature for uncoated Ti–6Al–4V

Group	Sintering treatment	Hydrogen-alloying treatment steps	Hydrogen (wt %)
A	1100 °C for 0.5 h	850 °C for 0.5 h	0.74 (0.05)
	1370 °C for 4 h	850 °C for 0.5 h	0.73 (0.11)
B	1100 °C for 0.5 h	850 °C for 0.5 h/ 590 °C for 4 h	0.50 (0.01)
	1370 °C for 4 h	850 °C for 0.5 h/ 590 °C for 4 h	0.65 (0.00)

(II) Effect of porous coating at constant sintering temperature of 1370 °C

Group	Sintering treatment	Hydogen-alloying treatment steps	Hydrogen (wt %)
C	Uncoated	850 °C for 0.5 h	0.75 (0.05)
	Porous coated	850 °C for 0.5 h	0.79 (0.03)
D	Uncoated	850 °C for 0.5 h/ 590 °C for 4 h	0.64 (0.03)
	Porous coated	850 °C for 0.5 h/ 590 °C for 4 h	0.65 (0.02)

Figures in parentheses are standard deviations.

instead of cooling to room temperature following hydrogenation.

Several of the specimens cracked during hydrogenation at 575 and 650 °C, even when slower cooling rates were employed. Therefore, cracking is more a function of hydrogen content than cooling rate. Based on the results of this study, keeping hydrogen concentrations < 1.5 wt % will avoid cracking. Weight percentages < 1.5 wt % are best attained by using hydrogenation temperatures > 650 °C.

During thermal treatment of titanium alloys, α-case may form. The thickness of the α-case varies with treatment temperature and time, and ranges from several micrometres to several hundred micrometres [23, 24]. Hydrogenation treatments in a vacuum of 10^{-4} torr [25] yielded hydrogen concentrations similar to the concentrations obtained in this study. It can therefore be assumed that the oxygen enriched surface had no effect on hydrogenation. The oxide barrier may even be beneficial, since it can aid in the retention of the desired amount of hydrogen during cooling and subsequent treatments [11]. The oxygen enriched surface is important only because it affects the mechanical

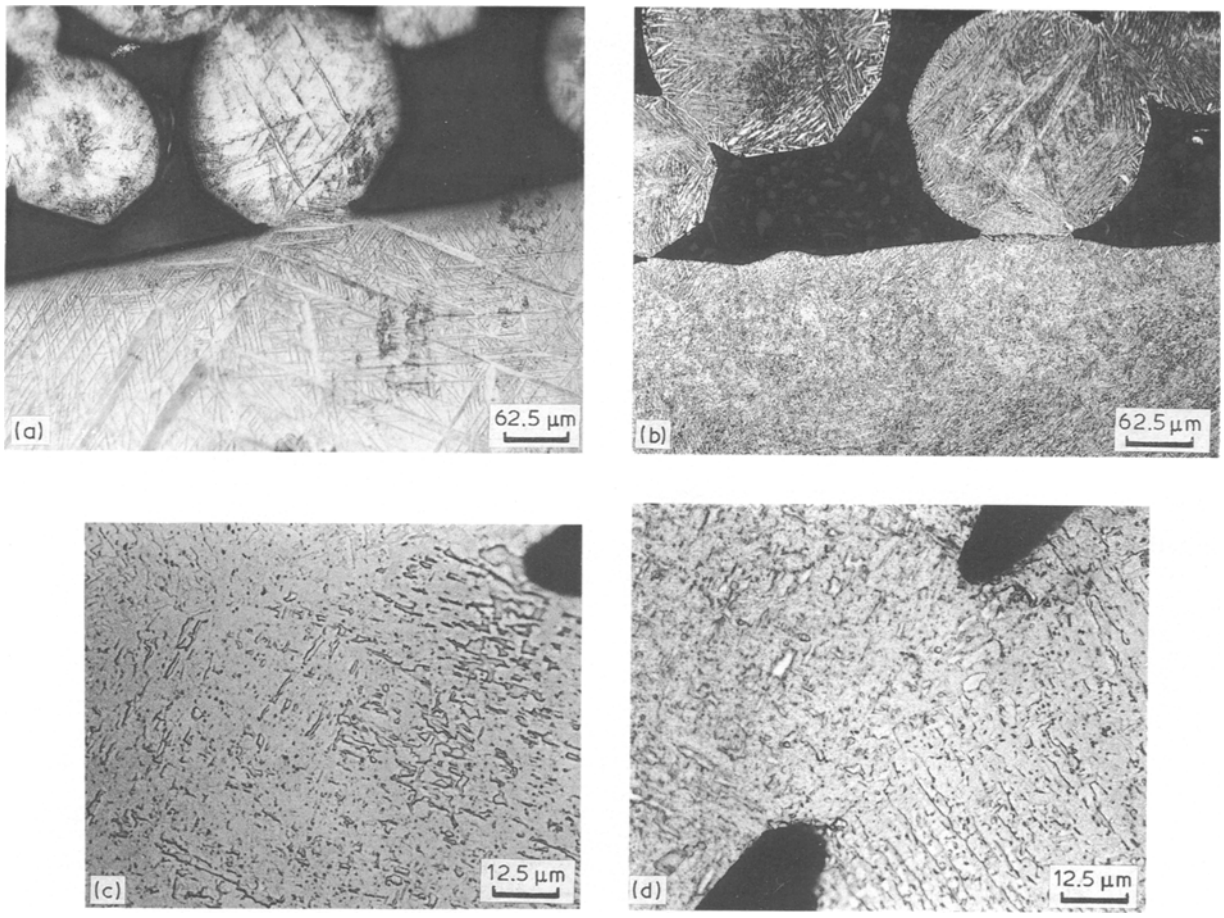

Figure 6 Light micrograph of porous-coated Ti–6Al–4V subjected to (a) hydrogenation (850 °C for 0.5 h), (b) hydrogenation–eutectoid decomposition (850 °C for 0.5 h in hydrogen/590 °C for 4 h in argon), (c) hydrogenation–dehydrogenation (850 °C for 0.5 h in hydrogen/650 °C for 16 h in vacuum) and (d) hydrogenation–eutectoid decomposition–dehydrogenation (850 °C for 0.5 h in hydrogen/590 °C for 4 h in argon/775 °C for 2 h in vacuum).

properties of the treated material. However, if the treated component is not in final form, treatments need not be conducted in vacuum.

The post-sintered lamellar microstructure consisted of α-platelets in a β-matrix, with GBα (Fig. 1). Hydrogenation at 800 °C resulted in a mostly single-phase β-microstructure, containing titanium hydride (γ) needles (Fig. 2b). The hydrogenated β-phase is denoted as β_H. Isolated platelets of (α + β) were also present. In view of the limited number of (α + β) platelets retained following hydrogenation at 800 °C, this temperature must be close to, or above, the β_H-transition temperature for hydrogen concentrations of 0.76 to 0.85 wt %.

Hydrogenation at 725 °C yielded 1.02 to 1.16 wt % hydrogen, but did not transform the (α + β) microstructure (Fig. 2a). Therefore, 725 °C is below the β_H-transformation temperature. Hydrogenation at 850 °C yielded a fully transformed β_H microstructure (Fig. 2c). The thicker white platelets indicate a breakup of the (α + β) platelets which existed following hydrogenation at 800 °C. Therefore, hydrogen reduced the β-transformation temperature from 975 °C at 0 % hydrogen to 800 to 850 °C at 0.71 to 0.85 wt % hydrogen, and enabled a phase transformation to a fully β_H microstructure to occur. This agrees with the findings of Kerr *et al.* [11], who reported that the β_H-transition remains constant at 800 °C for hydrogen concentrations >0.5 wt %. The extent of β_H-transformation depends on the temperature and hydrogen content, whereas the time and hydrogen content dictate the homogeneity and morphology of the microstructure.

The needles seen in Fig. 2 are termed line markings, and are thought to be precipitated from the γ-phase at low temperatures [26, 27]. The number and size of line markings depends on the amount of hydride, and may be used as a qualitative measure of hydrogen concentration [26].

The line markings were smaller in length following hydrogenation at 850 °C than at 800 °C. This can be explained by the fact that the solubility of hydrogen in β-titanium is high [28] and, during hydrogenation, hydrogen preferentially diffused into the β-phase. The titanium hydride phase is an ordered compound, which is formed when the hydrogen concentration reaches a threshold level for saturation of the β-crystal [29]. The results of this study indicate that the β_H hydrogen saturation level is 0.7 to 0.8 wt % (33 at %). The concentration of hydrogen in-diffused at 850 °C was closer to the threshold concentration for hydride formation and therefore, there were less line markings than at 800 °C.

On the basis of the concentration of hydrogen in-diffused and the transformed microstructure, 850 °C for 0.5 h was the best hydrogenation treatment and was used as the first step in all subsequent treatments.

Since a fully β_H microstructure is attained during hydrogenation, hydrogenation and β-transformation are combined into one step, yielding a more efficient treatment.

4.2. Eutectoid decomposition

Eutectoid decomposition treatments at 590 °C in a hydrogen environment (Table III) resulted in continued hydrogen in-diffusion beyond the hydrogen saturation concentration for 850 °C. The resultant microstructure was characterized by the nucleation of "black plates" at the prior β_H-grain boundaries (Fig. 3). Titanium alloys containing β-eutectoid elements nucleate two types of eutectoid-α: normal α and "black plates". The kinetics of "black plate" formation are more rapid than the kinetics of normal α precipitation, and therefore "black plate" formation occurs first [30]. Because of the high hydrogen concentrations (1.68 to 1.84 wt %), only "black plates" were formed in the allotted treatment times.

Eutectoid decomposition in an argon environment resulted in 0.24 to 0.39 wt % hydrogen removal and hydrogen concentrations were in the range 0.35 to 0.50 wt % for all eutectoid treatments performed in argon environments.

Treatments in which specimens were cooled to 590 °C, but not treated at 590 °C, also resulted in 0.50 wt % hydrogen. This result leads to the conclusion that most hydrogen evolution occurred during cooling from the hydrogenation temperature to the eutectoid temperature. Therefore, the eutectoid treatments at 590 °C were performed at almost constant hydrogen concentrations. Performing eutectoid treatments at constant and uniform hydrogen concentrations is important in obtaining a uniform microstructure.

Eutectoid treatments at hydrogen concentrations of 0.50 wt % promoted nucleation of eutectoid-α at the prior β_H-grain boundaries via a solid-state eutectoid decomposition reaction: $\beta_H(+\gamma) \rightarrow \alpha + \beta'_H(+\gamma)$. The symbol β'_H is used to denote the β-phase of the eutectoid microstructure, believed to be different, at least in composition, from the pretransformed β-phase, β_H. The resultant microstructures (Fig. 4a) were very fine two-phase ($\alpha + \beta'_H$) structures. Some γ may remain at the β_H-grain boundaries [12], depending on the local hydrogen concentrations. At the specimen periphery, a more acicular microstructure existed, with little of the β_H-phase remaining. Since measurable α-grain growth does not occur at 590 °C, the surface hydrogen concentration must be lower than the bulk hydrogen concentration. As a result, a less than optimum eutectoid transformation reaction occurred there. Eutectoid treatments lasting 8 h also produced α-platelet elongation (Fig. 4b). Eutectoid decomposition with a lower hydrogen concentration (0.35 wt %), therefore leads to a coarser grain morphology, with elongated and thickened α-grains.

The eutectoid decomposition treatments which produced the finest microstructures were those performed at 0.5 to 0.8 wt % hydrogen. If hydrogen concentrations were < 0.5 wt % or > 1.6 wt %, or if treatment times were too long (>4 h), elongated platelets formed. This range of hydrogen concentrations which best refines the microstructure agrees with the temperature–time–transformation–hydrogen concentration diagrams that Kerr *et al.* [11] developed. Therefore, eutectoid decomposition treatments of 590 °C for 2 or 4 h were used for all subsequent dehydrogenation studies.

4.3. Dehydrogenation

Eutectoid transformation refines the microstructure, yet the remaining hydrogen (0.5 wt %) has to be removed to avoid mechanical property degradation. Residual hydrogen concentrations compromise the mechanical integrity, since hydrides can fracture and act as crack nuclei [29]. However, as long as concentrations are < 140 p.p.m. (0.014 wt %), there is no effect of hydrogen on dynamic properties [31]. Accordingly, the maximum allowable hydrogen concentration in wrought Ti–6Al–4V is 120 p.p.m. (0.012 wt %) [18].

By dehydrogenating the discs, parametric temperature–time relationships for dehydrogenation were established. Dehydrogenation occurred more readily at higher temperatures and at longer treatment times (Tables IV and V). The data for the different treatment times at 700 °C imply that most of the hydrogen (0.442 wt %) was removed during the first half hour of treatment, and only an additional 0.04 wt % was removed in the following 1.5 h of treatment. The slow removal of the remaining hydrogen may be due to an oxide coating acting as a barrier to hydrogen transport. Dehydrogenation temperatures and times must be chosen within the constraint of minimizing α-grain growth. Grain growth is minimized if shorter times are used, the opposite requirement of efficient dehydrogenation.

The residual hydrogen concentrations determined by weighing and gas analysis differed by 0.0072 to 0.0145 wt %. This difference indicates that weighing incorporates the weight of a surface oxide layer, which grew during each of the four thermal–thermochemical cycles (sintering, hydrogenation, eutectoid decomposition and dehydrogenation). Weighing therefore yields conservative estimates of the bulk hydrogen concentrations.

Three dehydrogenation treatments yielded near-acceptable hydrogen concentrations: (1) 650 °C for 16 h (Fig. 5a), (2) 800 °C for 2 h (Fig. 5b) and (3) 775 °C for 4 h (Fig. 5c). None of these treatments compromised the previously established microstructural refinement. The α-grain sizes for treatments (1), (2) and (3) are, respectively, 0.91, 1.17 and 1.26 μm, compared with values of 3.40 and 4.00 μm for the equiaxed and lamellar structures.

Following dehydrogenation at 650 °C, a refined and uniform ($\alpha + \beta$) microstructure, which resembled a broken-down Widmanstatten microstructure was obtained (Fig. 5a). The primary-α grains were rounded, with an aspect ratio near unity, resembling an equiaxed-α microstructure. The prior β_H-grain boundaries formed colony boundaries for the α-phase, which

nucleated preferentially from the prior β_H-grain boundaries during β_H and hydride decomposition. Dehydrogenation at 775 and 800 °C (Fig. 5b and c) produced morphologically similar microstructures to those obtained following dehydrogenation at 650 °C. The higher dehydrogenation temperature resulted in more α-grain thickening and elongation, and formation of continuous GBα.

Although raising the dehydrogenation temperature enabled treatment times to be reduced, two aspects of the resultant microstructure reduce fatigue crack initiation resistance: α-grain thickening and elongation, and formation of continuous GBα.

A dehydrogenation treatment at 650 °C was conceived as a means of combining the eutectoid decomposition and dehydrogenation steps. Since a two-phase hydrogenation–dehydrogenation treatment (850 °C for 0.5 h/650 °C for 16 h) resulted in a microstructure similar to those obtained by the hydrogenation–eutectoid decomposition–dehydrogenation treatments, a separate eutectoid decomposition step may not be necessary. However, the intermediate 590 °C treatment may act as an ageing treatment to assure microstructural homogeneity [27]. Ageing also resulted in the removal of approximately 0.25 wt % hydrogen, enabling dehydrogenation times to be shortened.

4.4. Effect of sintering temperature and porous coating

The application of hydrogen-alloying treatments to porous-coated prostheses introduces two variables that warrant consideration: the sintering temperature and the porous coating.

The sintering temperature does not influence the hydrogen-alloying treatment steps. Hydrogen in-diffusion was independent of the sintering temperature (Table VII) and hydrogenation following sintering at 1370 °C yielded the same platelet-like ($\beta_H + \gamma$) morphology seen following hydrogenation after sintering at 1100 °C. Although a greater amount of hydrogen was retained during eutectoid decomposition when the higher sintering temperature was used (Table VII), the hydrogen concentration was within the optimal range and the resultant microstructure was still a finely dispersed eutectoid-α microstructure. Hydrogenation above the β_H-transition temperature homogenizes the microstructure, eradicating any differences in the starting microstructure. Hydrogen-alloying treatments are therefore independent of the initial forming process and are effective for cast, rolled and powder materials [12, 17].

Hydrogenation of a porous surface is potentially different from hydrogenation of a dense material. Hydrogen diffuses preferentially into notched regions, due to the expanded lattice [32]. Because of the notch-like character of the porous surface, local hydrogen accumulations may be greater than hydrogen levels in the bulk metal. Secondly, the diffusion coefficient of hydrogen in pure titanium is greater than the diffusion coefficient of hydrogen in Ti–6Al–4V [33]. The possibility of elevated hydrogen levels in the porous coating thus potentiated less than ideal eutectoid transformations, and more importantly, the possibility of cracking.

The bulk hydrogen concentrations changed little with the addition of a porous coating (Table VII) and no cracks were detected in hydrogenated porous-coated specimens under SEM. Following hydrogenation the microstructure in the porous coating and at the porous coating–substrate interface exhibited the characteristic ($\beta_H + \gamma$) morphology and thin platelets (Fig. 6a). Qualitatively, there appeared to be more line markings in the porous coatings than in the substrate, implying preferential hydrogen diffusion into the coating.

The microstructure in the region of the porous coating closest to the substrate was similar to the substrate microstructure. Microstructural continuity is due to the fact that alloying elements diffused into the porous coating during sintering. This alloying was confirmed by energy-dispersive X-ray analysis, which showed depleted aluminium levels in the substrate surface region. The importance of alloying lies in the fact that changes in aluminium and vanadium concentrations will alter the β-transformation temperature, and possibly affect this treatment step.

After eutectoid decomposition, porous-coated specimens exhibited the characteristic broken-up Widmanstatten microstructure (Fig. 6b). There were elongated α-platelets at the edges of the powdered spheres and at the coating–substrate interface. The less than optimal eutectoid transformation was probably due to local variations in the hydrogen concentration.

Following dehydrogenation, the microstructures at the porous-coating–substrate interface were similar to the uniquely fine microstructures produced in the uncoated specimens, a class of microstructures previously unattainable in porous-coated Ti–6Al–4V. The microstructures following the HAT-1 and HAT-3 treatments are shown in Fig. 6c and d. Comparing these microstructures with the post-sintered lamellar microstructure (Fig. 1b), it is clear that the microstructures at the sinternecks, the regions of fatigue crack initiation, were completely refined.

There were only minimal differences in the results of each hydrogen-alloying treatment step between porous-coated and uncoated specimens. Therefore, the addition of a porous coating does not affect the parameters of the hydrogen-alloying treatment steps.

4.5. Summary of hydrogen-alloying treatments

The use of hydrogen as a temporary alloying element in titanium alloys is possible because of the high diffusivity of hydrogen in titanium. Hydrogen is a β-eutectoid element. However, unlike most eutectoid reactions involving titanium systems, the Ti–H system has rapid transformation kinetics. It is known that upon decreasing the $(\alpha + \beta) \leftrightarrow \beta$ transformation temperature, nucleated α-colonies become smaller, contain fewer parallel platelets and nucleate independently of grain boundaries [34]. Therefore, microstruc-

ture lamellarity can be relieved in β-eutectoid systems.

In its most complete form the hydrogen-alloying treatment sequence consists of four steps: (1) hydrogenation ($(\alpha + \beta) \rightarrow \alpha + \beta_H + \gamma$), (2) β-transformation ($\alpha + \beta_H + \gamma \rightarrow \beta_H + \gamma$), (3) eutectoid decomposition ($\beta_H + \gamma \rightarrow \alpha + \beta'_H + \gamma$) and (4) dehydrogenation ($\alpha + \beta'_H + \gamma \rightarrow \alpha + \beta$). The critical aspects of each of the four steps are, respectively: (1) the concentration of hydrogen, (2) the extent of β_H-transformation, (3) the extent of eutectoid decomposition and the fineness of the decomposition product and (4) the removal of hydrogen with minimal α-grain growth and GBα precipitation.

Fig. 7 is a schematic (Ti–6Al–4V)–H phase diagram for the hydrogen concentrations and temperature ranges considered in this study. The broken lines reflect that the exact shape and position of the phase boundaries are not known. Also shown are the transformation reaction pathways for three variations of the hydrogen-alloying treatments: (1) HAT-1 (ABCDE), (2) HAT-2 (ABCFGH) and (3) HAT-3 (ABCFIJ).

For larger and more-complex components, such as total joint prostheses, longer hydrogenation times may be necessary to achieve hydrogen saturation conditions. Larger specimens may also require longer eutectoid decomposition treatment times. In light of the dependence of the treatment sequence on the component dimensions, the extent of microstructural refinement in joint prostheses may be less than in smaller specimens. It should be kept in mind, though, that the impetus for formulating these treatments was to achieve an improvement in fatigue strength. Since fatigue is primarily a surface-controlled phenomenon, it is important to achieve microstructural refinement at the surface but not necessarily in the bulk.

The final evaluation of the hydrogen-alloying treatments comes from fatigue testing. The results of tensile and fatigue testing are presented in companion papers [16, 35].

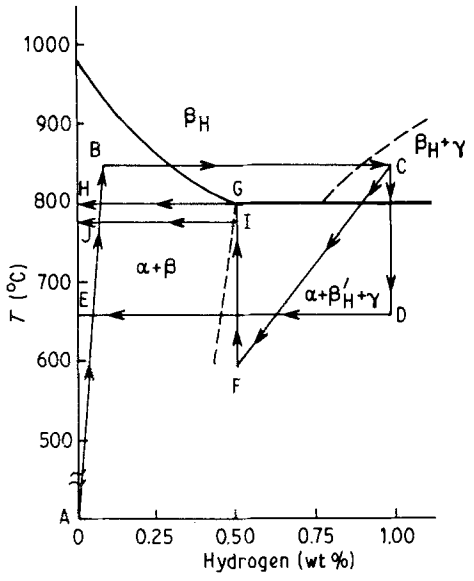

Figure 7 Schematic of proposed (Ti–6Al–4V)–H phase diagram and transformation pathways: HAT-1, ABCDE; HAT-2, ABCFGH; HAT-3, ABCFIJ.

In summary, the following conclusions are drawn.

1. Post-sintering hydrogen-alloying treatments can reverse microstructural lamellarity in β-sintered and porous-coated Ti–6Al–4V. The resultant microstructures can have α-grain sizes < 1 μm, aspect ratios near unity and discontinuous GBα, microstructural attributes which increase the fatigue strength.

2. Microstructural refinement occurs because hydrogen-alloying reduces the $(\alpha + \beta) \leftrightarrow \beta$ transition temperature and enables a eutectoid decomposition reaction to occur.

(a) The optimal hydrogenation temperature is 850 °C, because hydrogen concentrations of 0.71 to 0.85 wt % are in-diffused and β_H-transformation is achieved. These weight percentages are in the optimal range for efficient eutectoid decomposition kinetics and β_H-transformation obviates the need for a separate β_H-transformation treatment step.

(b) A separate eutectoid decomposition treatment step may be used, or eutectoid decomposition may be combined with dehydrogenation. The finest eutectoid microstructures are obtained if hydrogen concentrations are in the range 0.5 to 0.8 wt %.

(c) The criteria for dehydrogenation are efficient removal of hydrogen, with minimal grain growth and absence of GBα. These criteria are best met by using dehydrogenation temperatures < 700 °C.

3. Altering the sintering temperature or adding a porous coating does not affect the parameters of the hydrogen-alloying treatment steps.

Acknowledgement

This study was made possible by a grant in aid from DePuy, Inc., Warsaw, Indiana 46580.

References

1. C. A. STUBBINGTON, *AGARD Conf. Proc. No. 185* (1976) 3.1.
2. H. MARGOLIN, J. C. WILLIAMS, J. C. CHESNUTT and G. LUTJERING, in "Titanium '80 Science and Technology", Proceedings of the 4th International Conference on Titanium, Kyoto, May 1980, edited by H. Kimura and O. Izumi (Metallurgical Society of AIME, Warrendale, Pennsylvania, 1980) p. 169.
3. M. PETERS, A. GYSLER and G. LUTJERING, *ibid.* p. 1777.
4. G. LUTJERING and A. GYSLER, in "Titanium, Science and Technology", Proceedings of the 5th International Conference on Titanium, Munich, September 1984, edited by G. Lutjering, U. Zwicker and W. Bunk (Deutsche Gesellschaft für Metallkunde, Oberursel, 1985) p. 2065.
5. J. C. CHESNUTT, C. G. RHODES and J. C. WILLIAMS, ASTM STP 600 (ASTM, Philadelphia, 1976) p. 99.
6. R. E. LEWIS, J. G. BJELETICH, T. M. MORTON and F. A. CROSSLEY, ASTM STP 601 (ASTM, Philadelphia, 1976) p. 371.
7. J. J. LUCAS and P. P. KONIECZNY, *Met. Trans.* **2** (1971) 911.
8. C. A. STUBBINGTON and A. W. BOWEN, *J. Mater. Sci.* **9** (1974) 941.
9. S. M. SOLTESZ, R. J. SMICKLEY and L. E. DARDI, in "Titanium, Science and Technology", Proceedings of the 5th International Conference on Titanium, Munich, September 1984, edited by G. Lutjering, U. Zwicker and W. Bunk (Deutsche Gesellschaft für Metallkunde, Oberursel, 1985) p. 187.

10. J. GALANTE, W. ROSTOKER, R. LUECK and R. D. RAY, *J. Bone Joint Surg.* **53A** (1971) 101.
11. W. R. KERR, P. R. SMITH, M. E. ROSENBLUM, F. J. GURNEY, Y. R. MAHAJAN and L. R. BIDWELL, in "Titanium '80 Science and Technology", Proceedings of the 4th International Conference on Titanium, Kyoto, May 1980, edited by H. Kimura and O. Izumi (Metallurgical Society of AIME, Warrendale, Pennsylvania, 1980) p. 2477.
12. L. LEVIN, R. G. VOGT, D. EYLON and F. H. FROES, in "Titanium, Science and Technology", Proceedings of the 5th International Conference on Titanium, Munich, September 1984, edited by G. Lutjering, U. Zwicker and W. Bunk (Deutsche Gesellschaft für Metallkunde, Oberursel, 1985) p. 2107.
13. D. EYLON, C. F. YOLTON and F. H. FROES, in "Titanium Science Technology and Applications", Proceedings of the 6th World Conference on Titanium, Cannes, June 1988, edited by P. Lacombe, R. Tricoy and G. Beranger (Les Editions de Physique, Paris, 1989) p. 1523.
14. C. F. YOLTON, D. EYLON and F. H. FROES, *ibid.* p. 1641.
15. D. H. KOHN and P. DUCHEYNE, in Transactions of the 15th Annual Meeting of the Society for Biomaterials, Orlando, May 1989, p. 155.
16. *Idem., J. Mater. Sci.* submitted.
17. W. H. KAO, D. EYLON, C. F. YOLTON and F. H. FROES, in "Progress in Powder Metallurgy", Vol. 37 (MPIF, Princeton, New Jersey, 1981) p. 289.
18. ASTM Standard F136-84, in "Annual Book of ASTM Standards", Vol. 13.01: "Medical Devices" (ASTM, Philadelphia, 1987) p. 28.
19. ASTM Standard E112-85, in "Annual Book of ASTM Standards", Vol. 3.01: "Metals—Mechanical Testing; Elevated and Low-temperature Tests; Metallography" (ASTM, Philadelphia, 1988) p. 277.
20. L. S. DARKEN and R. W. GURRY, "Physical Chemistry of Metals" (McGraw-Hill, New York, 1953).
21. R. J. WASILEWSKI and G. L. KEHL, *Metallurgia* **50** (1954) 225.
22. R. G. VOGT, D. EYLON and F. H. FROES, US Patent 4 680 063 (1987).
23. ASM Committee on Titanium and Titanium Alloys, in "Titanium and Titanium Alloys Source Book", edited by M. J. Donachie, Jr (ASM, Metals Park, Ohio, 1981) p. 330.
24. D. J. HAGEMAIER, in "Titanium Science and Technology", Proceedings of the 2nd International Conference on Titanium, Cambridge, Massachusetts, May 1972, edited by R. I. Jaffee and H. M. Burte (Plenum Press, New York, 1973) p. 755.
25. R. J. SMICKLEY and E. DARDI, US Patent 4 505 764 (1985).
26. C. M. CRAIGHEAD, G. A. LENNING and R. I. JAFFEE, *J. Met.* **194** (1952) 1317.
27. G. A. LENNING, C. M. CRAIGHEAD and R. I. JAFFEE, *J. Met.* **200** (1954) 367.
28. M. HANSEN, "Constitution of Binary Alloys" (McGraw-Hill, New York, 1958).
29. N. E. PATON and J. C. WILLIAMS, in "Hydrogen in Metals: Proceedings of an International Conference on the Effects of Hydrogen on Materials Properties and Selection and Structural Design", edited by I. M. Bernstein and A. W. Thompson (ASM, Metals Park, Ohio, 1974) p. 409.
30. E. S. K. MENON and H. I. AARONSON, *Acta Metall.* **34** (1986) 1963.
31. C. J. BEEVERS, in "The Science, Technology and Application of Titanium", Proceedings of the 1st International Conference on Titanium, London, May 1968, edited by R. I. Jaffee and N. E. Promisel (Pergamon Press, London, 1968) p. 535.
32. V. KERLINS, in "Metals Handbook", 9th Edn, Vol. 12: "Fractography" (ASM, Metals Park, Ohio, 1979) p. 12.
33. U. ZWICKER, "Titan und Titanlegierungen" (Springer-Verlag, Berlin, 1974).
34. C. HAMMOND and J. NUTTING, *Met. Sci.* (1977) 474.
35. D. H. KOHN and P. DUCHEYNE, *J. Biomed. Mater. Res.* in press.

Received 26 October
and accepted 8 November 1989